Research Article

Alexey Pechenkin*, Dmitry Potemkin, Sukhe Badmaev, Ekaterina Smirnova, Kirill Cherednichenko, Vladimir Vinokurov, and Aleksandr Glotov

CO_2 hydrogenation to dimethyl ether over In_2O_3 catalysts supported on aluminosilicate halloysite nanotubes

https://doi.org/10.1515/gps-2021-0058
received June 14, 2021; accepted September 01, 2021

Abstract: This work presents results on CO_2 hydrogenation to dimethyl ether (DME) over bifunctional catalysts consisting of In_2O_3, supported on natural clay halloysite nanotubes (HNT), and HNT modified with Al-MCM-41 silica arrays. The catalysts were characterized by TEM, STEM, EDX-mapping, NH_3-TPD, XRD, low-temperature nitrogen adsorption, TPO, and H_2-TPR techniques. Catalytic properties of In_2O_3/HNT and In_2O_3/Al-MCM-41/HNT in the CO_2 hydrogenation to DME were investigated in a fixed-bed continuous flow stainless steel reactor at 10–40 atm, in the temperature range of 200–300°C, at GHSV = 12,000 h^{-1} and molar ratio of H_2:CO_2 = 3:1. The best catalyst for CO_2 hydrogenation was In_2O_3/Al-MCM-41/HNT that provided DME production rate 0.15 $g_{DME}\cdot(g_{cat}\cdot h)^{-1}$ with DME selectivity 53% and at 40 bar, GHSV = 12,000 h^{-1}, and T = 250°C. It was shown that In_2O_3/Al-MCM-41/HNT exhibited stable operation for at least 40 h on stream.

Keywords: CO_2 hydrogenation, dimethyl ether, indium oxide catalysts, halloysite nanotubes, mesoporous aluminosilicates

*** Corresponding author: Alexey Pechenkin,** Department of Physical and Colloid Chemistry, Gubkin Russian State University of Oil and Gas, 65 Leninsky prosp., 119991 Moscow, Russia; Boreskov Institute of Catalysis, Pr. Akademika Lavrentieva, 5, 630090, Novosibirsk, Russia, e-mail: pechenkin@catalysis.ru
Dmitry Potemkin: Boreskov Institute of Catalysis, Pr. Akademika Lavrentieva, 5, 630090, Novosibirsk, Russia; Novosibirsk State University, Pirogova St., 2, Novosibirsk 630090, Russia; Department of Environmental Engineering, Novosibirsk State Technical University, Karl Marx Pr., 20, 630073, Novosibirsk, Russia
Sukhe Badmaev: Boreskov Institute of Catalysis, Pr. Akademika Lavrentieva, 5, 630090, Novosibirsk, Russia
Ekaterina Smirnova, Kirill Cherednichenko, Vladimir Vinokurov, Aleksandr Glotov: Gubkin Russian State University of Oil and Gas, 65 Leninsky prosp., 119991 Moscow, Russia

1 Introduction

Currently, many efforts of various researchers around the world are being made to solve environmental problems. Air pollution is considered one of the main such problems. Various options are offered – the use of alternative energy sources, such as solar [1], wind [2], and biofuel [3]. However, it is also necessary to pay great attention to the utilization of CO_2. The ever-growing production capabilities of different countries lead to an increase in carbon dioxide emissions into the atmosphere. This is the reason for the increase in the so-called "greenhouse effect," which leads to an increase in the global temperature of the planet and, accordingly, climate change. This, as well as the fact that CO_2 is an inexpensive, readily available compound, requires the search for new technologies, methods, and ways of processing carbon dioxide. Recently, more and more attention of researchers from all over the world has been attracting the study of the reaction of CO_2 hydrogenation into various compounds such as methane [4], methanol [5–8], dimethyl ether (DME) [9–11], or hydrocarbons [12]. Among these compounds, DME attracts attention as a multipurpose product – it is used in the synthesis of methyl acetate, dimethyl sulfate, various petrochemical compounds, as a feedstock for powering fuel cells [13–15]. Due to its properties – high cetane number (55–60), low autoignition temperature, and high oxygen content (~35%), DME is considered as an alternative to diesel fuel or LPG. In terms of its physicochemical properties, DME is close to LPG, which allows its simple storage and transportation.

Commonly, DME is synthesized according to a two-stage scheme through the synthesis of methanol (MeOH) from synthesis gas on $Cu/ZnO/Al_2O_3$ (CZA) catalyst and its subsequent conversion into DME on a solid acid catalyst. However, the direct synthesis of DME is thermodynamically more favorable than the synthesis of methanol [16], which attracts more attention to the study of this

process. Catalysts for the direct synthesis of DME by hydrogenation of CO_2 are divided into two types: first, a mechanical mixture of catalysts for the synthesis of methanol and a catalyst for its dehydration; second, a catalyst called "bifunctional" which contains both types of necessary catalytic sites on its surface. Typically, first type systems are prepared by mixing or grinding of methanol synthesis and acidic components. Such method has some disadvantages like disintegration of its components during the reaction, mass, and heat transfer limitations [17]. So, recently, bifunctional catalysts have attracted much attention of scientists [10]. Another challenge is to perform direct DME synthesis with high selectivity without formation of CO. Industrial $Cu/ZnO/Al_2O_3$ methanol synthesis catalyst is also known to be active in reverse water gas shift (RWGS) reaction causing hydrogen losses due to formation of CO.

According to the recent density functional theory calculations [18], it is possible to obtain methanol with high selectivity via the hydrogenation of CO_2 on indium oxide. The reaction proceeds by the cyclic mechanism of the formation of oxygen vacancies and subsequent activation of CO_2 on them. Later, these calculations were experimentally confirmed. It was shown that methanol with ~100% selectivity is achieved on bulk In_2O_3 at low CO_2 conversions [19]. These works gave an impetus to further extensive studying of catalysts on indium oxide in the hydrogenation of CO_2 – the effect of various supports, preparation methods, the structure of indium oxide, and various additives on the catalytic activity [20–24]. Thus, indium oxide as a catalyst for methanol synthesis looks promising. An acid component is required for the design of a bifunctional DME direct synthesis catalyst. Usually, γ-Al_2O_3 or various zeolites – H-ZSM-5, Y, MOR, FER – are used as an acid catalyst in a two-stage process [17,25–33].

In this work for the first time, halloysite aluminosilicate nanotubes (HNT) were used as an acid support for the direct synthesis of DME catalysts. Halloysite nanotubes (HNT) have a rolled tubular structure (length ~1–2 μm, inner diameter 10–30 nm) [34–37]. In particular, halloysite was successfully applied as a support for catalysts of various applications, including aromatics hydrogenation [38–42], DME conversion to olefins [43], hydrogen production [44], Fischer–Tropsch synthesis [45], xylene isomerization [46,47], catalytic cracking [48], photocatalysis [49,50], etc. Its feature is that HNT contains two different types of active centers – functional groups of SiO_2 are present on the surface of nanotubes, while Al_2O_3 groups are located inside. This surface chemistry allows the metal component to be applied to both the external and internal surfaces, depending on the desired properties.

Nowadays, core-shell structure catalysts, such as $Cu–ZnO–Al_2O_3$@HZSM-5 [51] or $CuO–ZnO–Al_2O_3$@$SiO_2–Al_2O_3$ [52], are intensively studying in direct DME synthesis from CO_2. These systems prevent metal particles from sintering [53] and deactivation due coke formation by side reactions [54]. So, in the literature there are works on the modification surface of halloysite with MCM-41 [36] to make core-shell structure. This core-shell halloysite – based aluminosilicate composite is promising for catalytic applications due to high specific surface area and enhanced thermal and mechanical properties [39]. However, pure MCM-41 doesn't have the required acid sites on its surface. Therefore, before using it as a support, the surface was modified with aluminum in order to increase acid sites. The resulting Al-MCM-41 has a large amount of acid sites, which are necessary to produce DME by CO_2 hydrogenation.

In this work, we present novel bifunctional In_2O_3 catalysts supported on natural clay nanotubes (10 wt% In_2O_3/HNT) and composite with structured mesoporous silica (10 wt% In_2O_3/MCM-41/HNT) for CO_2 hydrogenation to DME.

2 Experimental section

2.1 Synthesis and characterization of catalysts

As a support for catalysts, HNT (≥98%, Sigma-Aldrich, St. Louis, MO, USA) and ordered mesoporous composite Al-MCM-41/HNT were used. This modified support was prepared by the template synthesis method as described in literature [43]. Cetyltrimethylammonium bromide (≥98%, Sigma-Aldrich, St. Louis, MO, USA) was used for the formation of MCM-41. Aluminum isopropoxide (≥98%, Sigma-Aldrich, St. Louis, MO, USA) was used as an aluminum source. The weight ratio between Al-MCM-41 and HNT in the synthesized support was 60:40%.

In_2O_3/HNT and In_2O_3/Al-MCM-41/HNT catalysts were synthesized by the incipient wetness impregnation method of HNT and Al-MCM-41/HNT with aqueous solutions of indium nitrate(III) (Reakhim, Moscow, Russia, purity 99.99%) taken at desired ratio, respectively. The samples were dried at 80°C in air for 4 h and after that calcined at 400°C (heating rate 1°C·min^{-1}) for 3 h in air.

Actual In_2O_3 loadings in the catalysts were determined by inductively coupled plasma atomic emission spectrometry (Optima instrument; Perkin-Elmer).

Transmission electron microscope (TEM) JEOL JEM-2100 (UHR) operated at 200 kV (the lattice resolution of

0.19 nm) and equipped with LaB6 gun was employed to investigate structure, morphology, and chemical composition of the obtained samples. The samples for the TEM analysis were prepared by the dispersing in ethanol. The as-prepared dispersed solution was dropped onto carbon-coated formvar TEM Cu grid (300 mesh, Ted Pella, Inc.). The acquisition of TEM/HRTEM images was performed in TEM mode using Olympus Quemesa 11 megapixel CCD camera. The collection of each EDX map was performed in STEM mode with help of EX-24065JGT energy dispersive X-ray (EDX) analyser.

The specific BET surface areas (S_{BET}) and pore volume (V_p) of the support and the catalysts were determined using the low-temperature N_2-adsorption method using a TriStar3000 apparatus. Before experiment, all samples were outgassed in vacuum at 300°C, then nitrogen adsorption/desorption isotherms were recorded at –196°C. The specific surface area of the samples was calculated by the Brunauer–Emmett–Teller (BET) equation. The pore volume was evaluated in accordance with Barrett–Joyner–Halenda model.

NH_3 temperature-programmed desorption (NH_3-TPD) was used to evaluate the acid properties of the samples. The catalyst was saturated by mixture of NH_3 and N_2 at 100°C for 30 min. After that, the sample was purged with a stream of nitrogen to remove physisorbed ammonia at same conditions. Then NH_3-TPD curve was recorded up to 700°C with a rate of 10° per minute.

Temperature-programmed reduction (H_2-TPR) and temperature-programmed oxidation (TPO) experiments were carried out using a STA 409 PC Luxx derivatograph fitted with a QMS-200 mass spectrometer. For H_2-TPR, the samples (~50 mg) were heated from room temperature to 500°C (5°C·min^{-1}) in a 10 vol% H_2–Ar mixture flowing at 100 mL·min^{-1}. For TPO, samples were heated from 25°C to 800°C in a 10 vol% O_2–Ar mixture flowing at 100 mL·min^{-1}.

X-ray structural analysis (XRD) of the samples was recorded on a Bruker D8 Advance (Bruker, Germany) diffractometer (CuKα) in the 2θ range of 8°–63° with a step 0.05° per 4 s. Analysis of the obtained diffraction data was carried out using the PowderCell 2.4 programme using the JCPDS international diffraction database as a reference.

2.2 Catalyst testing

Catalytic experiments on CO_2 hydrogenation were studied in a fixed-bed continuous-flow stainless steel reactor (inner diameter 8 mm) at a 10–40 atm pressure in the temperature interval 200–300°C, at GHSV = 12,000 h^{-1} and molar ratio H_2:CO_2 = 3:1. Prior to the reaction, all the catalysts (V_{cat} = 2 cm^3, m_{cat} = ~1.4 g for In_2O_3/HNT and ~0.5 g for In_2O_3/Al-MCM-41/HNT, particle size of 0.5–1 mm) were pretreated at 300°C for 1 h in helium flow. The temperature was measured using a chromel-alumel thermocouple, which was placed in the middle of the catalytic bed. The results were obtained after multiple catalytic experiments. The catalysts were tested in several temperature increasing/decreasing cycles. At each temperature, the catalyst was kept for 1–2 h. Thus, total time onstream under CO_2 hydrogenation conditions was not less than 10 h. The catalytic performance during this period remained stable. The compositions of the inlet and outlet gas mixtures were analyzed by a gas chromatograph (Chromos-1000) equipped with TCD and FID detectors and molecular sieve (5A) and Carbowax columns. Argon was used as a carrier gas. The detection limits for CO, CO_2, CH_4, DME, and methanol were 5×10^{-3} vol%. The carbon imbalance in all catalytic experiments was ±5%.

CO_2 conversion (X_{CO_2}), MeOH, and DME selectivity (S_{MeOH}, S_{DME}) were calculated as follows:

$$X_{CO_2}\ (\%) = \frac{C_{CO} + C_{CH_4} + C_{MeOH} + 2 \times C_{DME}}{C_{CO} + C_{CH_4} + C_{MeOH} + 2 \times C_{DME} + C_{CO_2}} \times 100 \quad (1)$$

$$S_{MeOH}\ (\%) = \frac{C_{MeOH}}{C_{CO} + C_{CH_4} + C_{MeOH} + 2 \times C_{DME}} \times 100 \quad (2)$$

$$S_{DME}\ (\%) = \frac{2 \times C_{DME}}{C_{CO} + C_{CH_4} + C_{MeOH} + 2 \times C_{DME}} \times 100 \quad (3)$$

$$W_{DME}\ (g_{DME} \cdot (g_{cat} \cdot h)^{-1}) = \frac{F_{DME} \times M_{DME}}{m_{cat}} \quad (4)$$

where C_i – outlet concentrations (vol%), F_i – flow rate (mol·h^{-1}), n_i – mole amount (mol), m – catalyst weight (g), M_i – molecular weight (g·mol^{-1}).

3 Results and discussion

3.1 Characterization of catalysts

The catalysts were characterized by TEM, STEM, EDX-mapping, NH_3-TPD, XRD, low-temperature nitrogen adsorption, TPO, and H_2-TPR techniques. The In_2O_3 loading, textural parameters, and structural data obtained from XRD patterns of fresh and used In_2O_3, In_2O_3/HNT, and In_2O_3/Al-MCM-41/HNT are presented in Table 1. We can see

Table 1: In_2O_3 loading, S_{BET}, pore volume, and coherent scattering region

Catalyst		Textural characteristics		In_2O_3	
		S_{BET} ($m^2 \cdot g^{-1}$)	V_p ($cm^3 \cdot g^{-1}$)	wt%	CSR[a] (nm)
HNT		71	0.16	—	—
MCM-41/HNT		514	0.42	—	—
In_2O_3	Fresh	68	0.41	100	13
10% In_2O_3/HNT	Fresh	62	0.13	9.12	16.5
	Used	61	0.13	9.12	16.4
10% In_2O_3/Al-MCM-41/HNT	Fresh	412	0.31	8.71	10.1
	Used	410	0.3	8.71	10.1

[a] CSR – coherent scattering region.

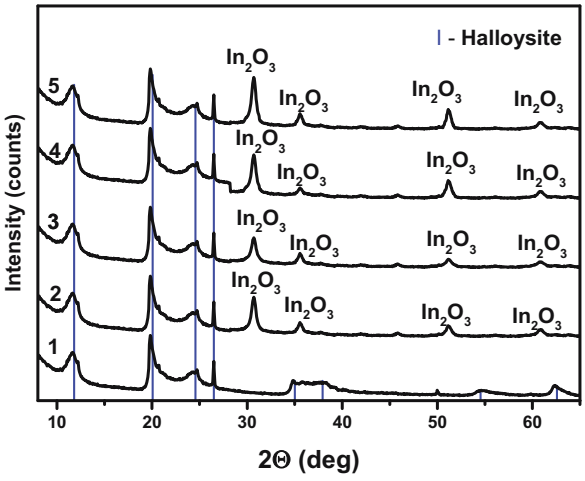

Figure 1: XRD patterns of catalysts. (1) halloysite, (2) In_2O_3/HNT fresh, (3) In_2O_3/HNT used, (4) In_2O_3/Al-MCM-41/HNT fresh, and (5) In_2O_3/MCM-41/HNT used.

that for the In_2O_3/HNT and In_2O_3/Al-MCM-41/HNT, real loadings of In_2O_3 are less than calculated. This is due to the fact that during impregnation supports absorbed lower volume of the indium nitrate water solution. The BET surface (Figure A1 in Appendix) areas of In_2O_3 and HNT are quite similar and equal 68 and 71 $m^2 \cdot g^{-1}$, respectively. After the impregnation of In_2O_3 on the HNTs' surface, morphological characteristics are practically unchanged: S_{BET} and pore volume slightly decreased to 62 $m^2 \cdot g^{-1}$ and 0.13 $cm^3 \cdot g^{-1}$, respectively. The most likely reason is blocking of some pores by the indium oxide particles.

Formation of MCM-41 phase on HNT leads to significant increase of surface area due to ordered structure of silica arrays. After deposition of indium oxide, specific surface area decreased by 100 $m^2 \cdot g^{-1}$, for the same reason as on the In_2O_3/HNT catalyst. Acidity parameters of the catalysts and supports calculated from NH_3-TPD method are listed in Table 2 (Figure A2). Based on the desorption spectra, the acidity was classified as weak and medium (amount of ammonia ($\mu mol \cdot g^{-1}$) desorbed below 300°C) and strong sites (amount of ammonia ($\mu mol \cdot g^{-1}$) desorbed above 300°C).

As shown in Table 2, the acidity of unmodified halloysite is seriously lower than that of HNT/Al-MCM-41 due to the fact that modified with aluminum MCM-41 has strong acid sites on the surface [43]. The total amount of acid sites on the surface of In_2O_3 supported catalysts is reduced in comparison with supports. This fact can be explained by partial blocking of the pores by the indium oxide particles. For the catalysts after the experiment, we can say that total amount of acid sites remained the same.

Figure 1 shows the XRD patterns for fresh and used catalysts. According to XRD data, we can say that indium oxide on the surface 10% In_2O_3/HNT has cubic crystal phase structure [21] with crystallite size of 13 nm. In case of 10% In_2O_3/Al-MCM-41/HNT, the crystallite size of the indium oxide is slightly smaller – 10 nm. We assumed that this is due to the higher dispersion of indium oxide particles. As we can see from the diffraction patterns of the used catalysts (curve 3 and 5 on Figure 1), there are no significant changes in the number and composition of the peaks. We only note that for the used catalysts, the

Table 2: Acidity properties of catalysts and supports

Sample	Acidity parameters		
	Weak and medium acid sites ($\mu mol \cdot g^{-1}$)	Strong acid sites ($\mu mol \cdot g^{-1}$)	Total acidity ($\mu mol \cdot g^{-1}$)
HNT	22	122	144
Al-MCM-41/HNT	35	495	530
10% In_2O_3/HNT	17	98	115
10% In_2O_3/Al-MCM-41/HNT	31	451	482

peaks related to indium oxide are slightly smaller compared to fresh catalysts. Both used catalysts don't have any considerable changes in the crystal structure – pore volume and CSR remained almost the same. This tells us that indium oxide particles are stable on the catalysts surface.

The In_2O_3/HNT and In_2O_3/Al-MCM-41/HNT catalysts were studied by TEM, STEM, and EDX techniques. Figure 2 shows the TEM images of the fresh and used catalyst In_2O_3/Al-MCM-41/HNT, which are obviously similar.

HNT were observed in both samples, and the images show that the nanotubes remained stable under reaction conditions. The same results were obtained for the In_2O_3/HNT catalyst. Also, in Figure 2b and d, we can see the structure of the mesoporous MCM-41 type silica deposited on the outer surface of HNTs. Some agglomerates of fresh and used In_2O_3/Al-MCM-41/HNT catalysts were studied by STEM and EDX-mapping. Results are shown in Figure 3. It is seen that the STEM images (Figure 3c and d) of both catalysts are similar. It can be noted that the indium particles are located mainly in the same place as the silicon particles in the case of both catalysts. Thus, it can be concluded that In_2O_3/Al-MCM-41/HNT catalyst contains two types of active sites on the surface – indium oxide particles, supported on silica, and alumina oxide particles.

Catalysts were examined by H_2-TPR (Figure 4) to study reducibility of catalysts. We can see that pure indium oxide isn't reduced in the investigated temperature range. For the In_2O_3/Al-MCM-41-HNT, hydrogen consumption occurs only at ~170°C, indicating that the indium oxide nanoparticles are mainly localized on mesoporous silica of Al-MCM-41 type. This peak can be correlated to reduction of In_2O_3 surface and can also be attributed as indirect evidence of the formation of oxygen vacancies on the surface of indium oxide [57,58]. For the In_2O_3/HNT, there is also a peak at ~170, which could be assigned to reduction of In_2O_3 surface particles on the outer (SiO_2) tubes surface as for the In_2O_3/Al-MCM-41/HNT. Calculation of H_2-consumption over In_2O_3/Al-MCM-41/HNT shows us that 20% of In_2O_3 loading was reduced. In the case of In_2O_3/HNT, there are 16% In_2O_3 on 170°C peak. So, in In_2O_3/Al-MCM-41/HNT, a higher amount of surface active indium oxide is observed.

Based on the data obtained, it can be concluded that the 10% In_2O_3/HNT and 10% In_2O_3/Al-MCM-41/HNT catalysts contain two types of sites on their surface – In_2O_3 particles as a metal component for the synthesis of methanol and acidic sites of HNT or Al-MCM-41/HNT for its further dehydration to DME.

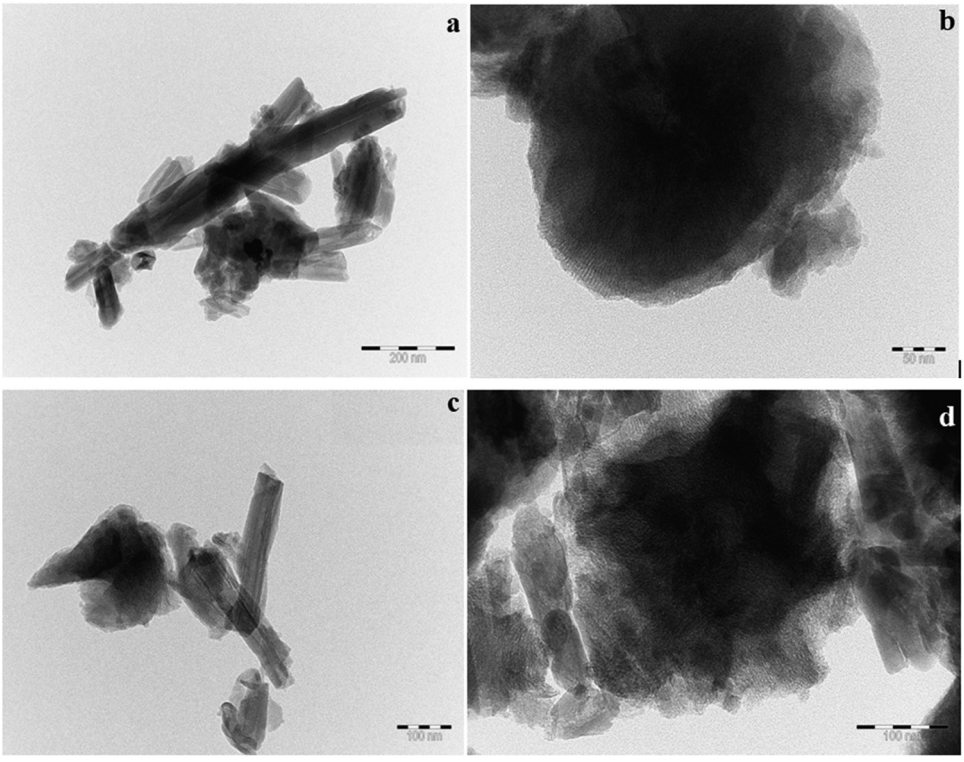

Figure 2: TEM images of fresh (a and b) and used (c and d) In_2O_3/Al-MCM-41/HNT catalyst.

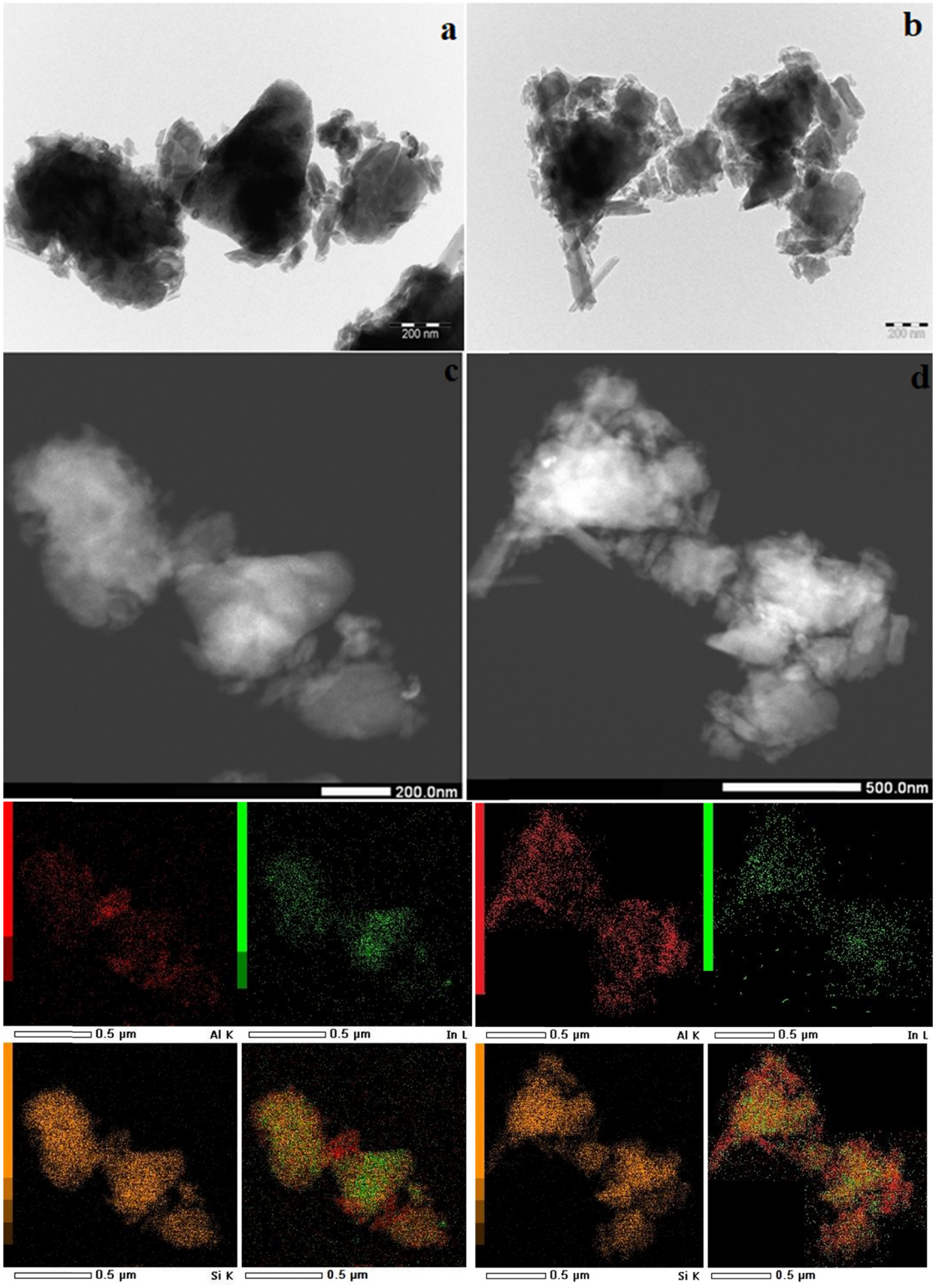

Figure 3: TEM images (a,c), STEM images (b,d) and the corresponding Al, Si and In mapping of fresh (a,c) and used (b,d) In_2O_3/Al-MCM-41/HNT catalyst.

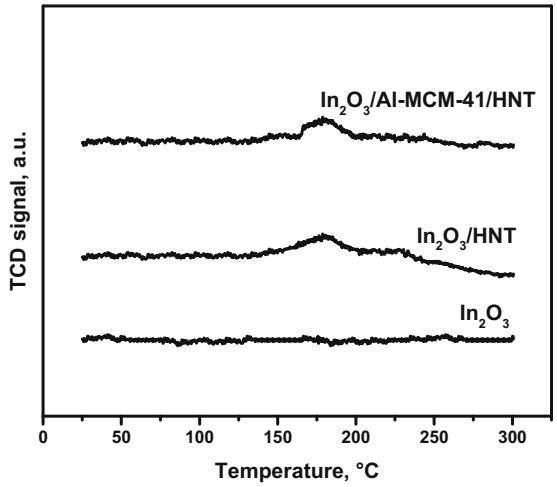

Figure 4: H_2-TPR profiles of fresh In_2O_3/HNT and In_2O_3/Al-MCM-41/HNT catalysts.

3.2 Catalytic results

The catalytic properties of the In_2O_3, 10% In_2O_3/HNT, and 10% In_2O_3/Al-MCM-41/HNT in CO_2 hydrogenation samples were measured at T = 200–300°C, P = 10–40 atm, and GHSV = 12,000 h^{-1}, respectively. Figure 5 shows temperature dependencies of CO_2 conversion and selectivity to MeOH (Figure 5a) and DME (Figure 5b) for In_2O_3, In_2O_3/HNT, and In_2O_3/Al-MCM-41/HNT catalysts. Only CO, H_2O, CH_3OH, and DME were detected as products; no hydrocarbons were identified.

Among the tested catalysts, In_2O_3 catalyst exhibited the lowest CO_2 conversion, but the highest methanol selectivity over the entire temperature range. This can be explained by the fact that no DME was observed in reaction products. It seems to be quite obvious, since this catalyst does not have required acid sites on its surface. We can see that CO_2 conversion increases with increasing temperature from 1% at 200°C up to 4% at 300°C. The selectivity for methanol, on the contrary, decreases with increasing temperature from 99% at 200°C to 65% at 300°C due to the CO formation by RWGS reaction.

In contrast to bulk In_2O_3 for the supported In_2O_3/HNT and In_2O_3/Al-MCM-41/HNT catalysts, DME appears in reaction products, due to the presence of acid sites. Temperature dependence for DME selectivity is similar to methanol in case of bulk In_2O_3 – the curve decreases with increasing temperature. There are some reasons for that. First, methanol dehydration is exothermic reaction, so increasing temperature leads to decrease of DME/MeOH equilibrium ratio. Second, at high temperatures, RWGS reaction (which is endothermic) contributes more to product distribution. So, it should be an optimal temperature, where the combination of formation rate of DME and CO_2 conversion will be maximum. Over the temperature range, we can see that on In_2O_3/Al-MCM-41/HNT there are higher values of CO_2 conversion and DME selectivity than on In_2O_3/HNT. Most likely, it is connected with higher surface area and more acid sites on In_2O_3/Al-MCM-41/HNT catalyst. Figure 6 shows temperature dependencies of DME production rate on In_2O_3, In_2O_3/HNT, and In_2O_3/Al-MCM-41/HNT catalysts.

The highest DME formation rate of 0.15 $g_{DME}\cdot(g_{cat}\cdot h)^{-1}$ was observed at 250°C on In_2O_3/Al-MCM-41/HNT. Further,

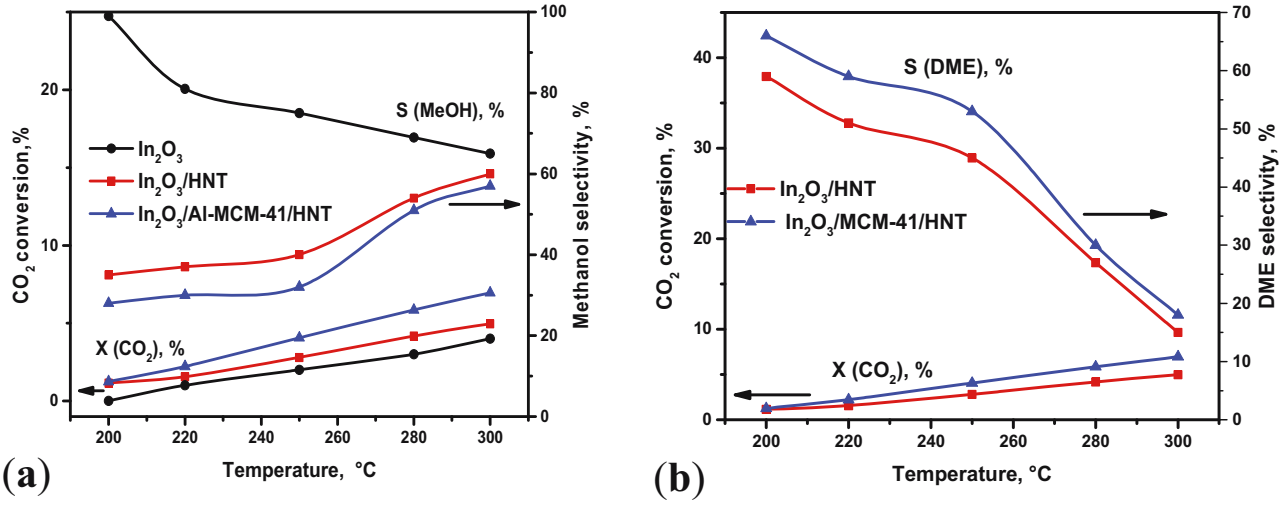

Figure 5: (a) Effect of temperature on CO_2 conversion and methanol selectivity over In_2O_3, In_2O_3/HNT, and In_2O_3/Al-MCM-41/HNT catalysts in CO_2 hydrogenation. (b) Effect of temperature on CO_2 conversion and dimethyl ether selectivity over In_2O_3/HNT and In_2O_3/Al-MCM-41/HNT catalysts in CO_2 hydrogenation. Reaction conditions: P = 40 atm, GHSV = 12,000 h^{-1}; inlet composition (vol%): H_2:CO_2 = 3:1.

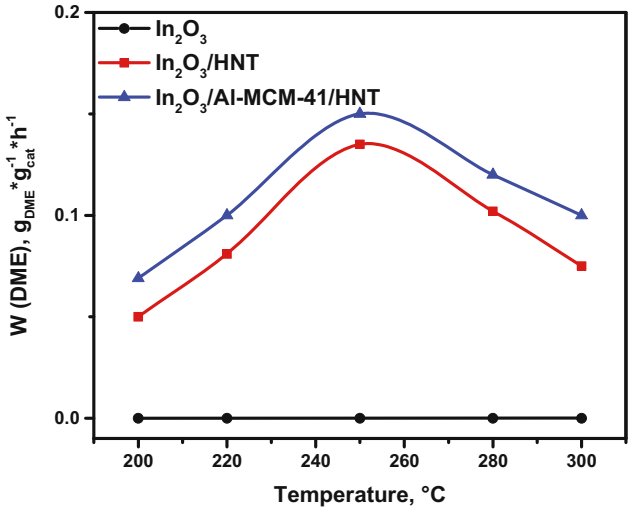

Figure 6: Effect of temperature on DME production rate over In_2O_3, In_2O_3/HNT, and In_2O_3/Al-MCM-41/HNT catalysts. Reaction conditions: P = 40 atm, GHSV = 12,000 h^{-1}; inlet composition (vol%):H_2:CO_2 = 3:1.

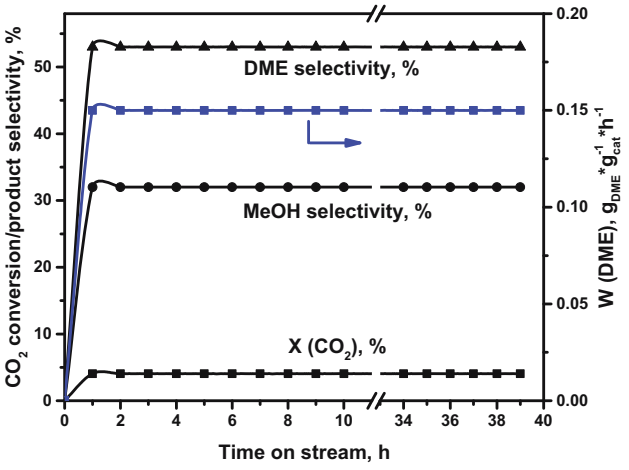

Figure 8: Effect of time on stream on CO2 conversion, methanol, and DME selectivity, DME production rate over In_2O_3/Al-MCM-41/HNT catalyst. Reaction conditions: T = 250°C, P = 40 atm, GHSV = 12,000 h^{-1}; inlet composition (vol%): H_2:CO_2 = 3:1.

the performance of the most active and selective catalyst In_2O_3/Al-MCM-41/HNT was studied in more detail.

It is well-known that with increasing pressure, the equilibrium of the CO_2 hydrogenation reaction shifts towards the products according to the Le Chatelier principle. So, we studied the pressure influence on catalytic activity in DME direct synthesis from CO_2 and H_2. The results are shown in the Figure 7. The experiments were carried out at T = 250°C, GHSV = 12,000 h^{-1}.

As expected, with increasing pressure, CO_2 conversion and DME selectivity also increase, while MeOH passes

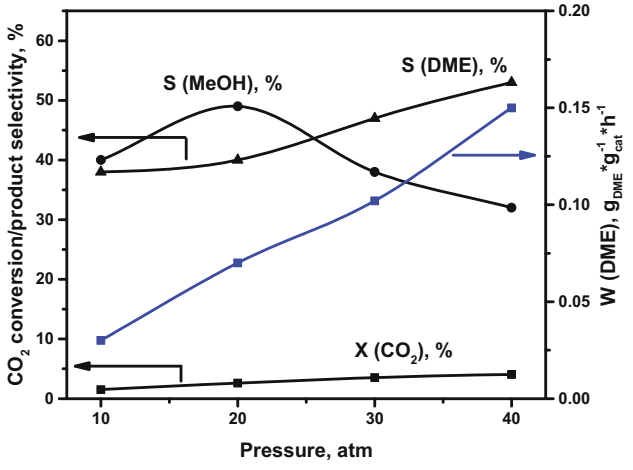

Figure 7: Effect of pressure on CO_2 conversion, methanol, and DME selectivity and DME production rate over In_2O_3/Al-MCM-41/HNT catalyst. Reaction conditions: T = 250°C, GHSV = 12,000 h^{-1}; inlet composition (vol%): H_2:CO_2 = 3:1.

through the maximum at 20 atm and then decreases. This is in accordance with thermodynamic equations for this system [9]. The highest value of the DME formation rate is observed at 4 MPa. Note that at temperatures higher than 250°C, W_{DME} decreased, despite an increase in the CO_2 conversion due to a significant drop of DME selectivity.

One of the key properties of the catalyst, in addition to activity, is the stability under reaction conditions. A series of experiments were carried out to investigate this aspect. Figure 8 shows the effect of time-on-stream on the outlet product concentrations and CO_2 conversion. The In_2O_3/Al-MCM-41/HNT catalyst was tested at 250°C, the inlet mixture H_2:CO_2 = 3:1, and GHSV = 12,000 h^{-1}. Under these conditions, only CO, MeOH, and DME were detected as reaction products; methane appeared only in trace amounts. During 10 h on stream, no significant changes were observed either in the conversion of CO_2 or in the MeOH and DME selectivity. No significant changes in the selectivity of DME were observed after 8 h of the experiment. After that, catalyst remained in operation conditions for 24 h, and after that catalyst activity was recorded. All the parameters, such as methanol, DME selectivity, and CO_2 conversion, remained the same. In our view, these results mean that indium oxide particles remained stable as well as acid sites of modified HNT. In addition, the spent catalyst was tested by TPO. No carbon deposition was observed. This means that acidic properties of HNT (strength and number of acidic sites) are optimal for DME synthesis reaction and do not induce condensation reactions.

Up to now, almost no works of using indium oxide for direct synthesis of DME can be found in literature; only

Table 3: Comparison of catalyst activities in CO_2 hydrogenation to dimethyl ether

Catalyst	*T* (°C)	Pressure (atm)	GHSV (mL·(g_{cat}·h)$^{-1}$)	*W* (DME) (g_{DME}·(g_{cat}·h)$^{-1}$)	Reference
In_2O_3/Al-MCM-41/HNT	250	40	12,000	0.15	This work
CIZO[1]/SAPO-34	250	30	6,000	0.08	[59]
CZA[2]/HZSM-5	260	30	1,500	0.12	[28]
CZZ[3]/ferrierite	260	50	8,800	0.435	[29]
CZA/HZSM-5	260	50	3,000	0.29	[30]
CZZ/MFI	240	50	10,000	0.251	[17]
CZZ/BEA	260	30	8,800	0.3	[31]
CZZ/WO_x–ZrO_2	260	30	4,333	0.27	[32]
PdZn/TiO_2-H-ZSM-5	270	20	3,500	0.025	[33]

[1] CuO-In_2O_3-ZrO_2; [2] CuO-ZnO-Al_2O_3; [3] CuO-ZnO-ZrO_2.

one work devoted to the study Cu–In–Zr–O catalyst mixed with SAPO-34 zeolite for direct DME synthesis is available [59]. Basically, all works on the direct synthesis of DME from CO_2 and H_2 are devoted to the study of copper catalysts mixed with zeolites. So, we compared the best In_2O_3/Al-MCM-41/HNT catalyst with literature data. Table 3 shows comparative data, in particular, experimental conditions (temperature, pressure, flow), CO_2 conversion, and DME selectivity. Since a fairly large number of works devoted to the hydrogenation of CO_2 to DME are currently presented in the literature, the table shows those with similar experimental conditions with this work, in particular – pressure of 10–50 atm, temperature of 200–300°C, and inlet composition H_2:CO_2 = 3:1.

Catalytic activity of In_2O_3/Al-MCM-41/HNT is lower than literature data, but study of these systems is at the very beginning. Such systems look very promising due to the following factors: the possibility of a significant increase in CO_2 conversion and selectivity for DME after optimization of the catalyst composition, its dispersion, the method of preparation, and adding of promoters. According to the literature data [60], catalysts based on indium oxide make it possible to obtain methanol with a selectivity of about 100%, and with the appropriate selection of the acid component, high DME yields can be achieved. It is also important that In_2O_3/MCM-41/HNT catalyst shows good stability, due to the fact that indium oxide particles do not sinter during the reaction, and acid sites remain stable in presence of water. There is a wide field for further catalyst improvement, including optimization of In_2O_3 morphology and interaction with the support, tuning acidic properties, doping by metals active in CO hydrogenation, such as Cu, Pd, Ga, and even Ni and Co. These points will be the subject of our further studies.

4 Conclusion

Indium oxide catalysts, bulk and supported on aluminosilicate HNTs and modified HNTs with ordered Al-MCM-41 silica arrays, were studied in CO_2 hydrogenation to DME. Based on data from physicochemical methods, such as XRD, S_{BET}, FTIR, and H_2-TPR, we can suggest that these catalysts have two types of active sites – indium oxide particles, which are responsible for methanol formation, and acid sites of HNT, which are responsible for methanol dehydration to DME. The influence of temperature and pressure was studied. The best catalyst for CO_2 hydrogenation was In_2O_3/Al-MCM-41/HNT that provides 4% CO_2 conversion with DME selectivity 53% and DME production rate 0.15 g_{DME}·(g_{cat}·h)$^{-1}$ at 40 bar, GHSV = 12,000 h^{-1}, and T = 250°C. It was shown that this catalyst didn't lose activity after 40 h of experiment. So, it is very promising systems, based on new material for direct hydrogenation of CO_2 to DME.

Funding information: This research was funded by RFBR project 19-33-60056 and as a part of the state task of Gubkin University (synthesis of MCM-41/HNT, textural properties evaluation, TEM), project number FSZE-2020-0007 (0768-2020-0007, A.G., V.V., K.Ch.).

Author contributions: Alexey Pechenkin: conceptualization, writing – original draft, writing – review and editing, methodology, formal analysis, investigation; Dmitry Potemkin: writing – review and editing, investigation, conceptualization, formal analysis; Sukhe Badmaev: resources, investigation; Ekaterina Smirnova: methodology, visualization; Kirill Cherednichenko: methodology, visualization, resources; Vladimir Vinokurov: writing – review and editing, project administration; Aleksandr Glotov: writing – review and editing, supervision.

Conflict of interest: Authors state no conflict of interest.

References

[1] Strielkowski W, Volkova E, Pushkareva L, Streimikiene D. Innovative policies for energy efficiency and the use of renewables in households. Energies. 2019;12(7):1392.

[2] Munters W, Meyers J. Dynamic strategies for yaw and induction control of wind farms based on large-eddy simulation and optimization. Energies. 2018;11(1):177.

[3] Gonçalves A, Puna JF, Guerra L, Campos Rodrigues J, Gomes JF, Santos MT, et al. Towards the development of syngas/biomethane electrolytic production, using liquefied biomass and heterogeneous catalyst. Energies. 2019;12(19):3787.

[4] Frontera P, Macario A, Ferraro M, Antonucci P. Supported catalysts for CO_2 methanation: a review. Catalysts. 2017;7:59.

[5] Graciani J, Mudiyanselage K, Xu F, Baber AE, Evans J, Senanayake SD, et al. Highly active copper-ceria and copper-ceria-titania catalysts for methanol synthesis from CO_2. Science. 2014;345:546–50.

[6] Kattel S, Ramírez PJ, Chen JG, Rodriguez JA, Liu P. Active sites for CO_2 hydrogenation to methanol on Cu/ZnO catalysts. Science. 2017;355:1296–9.

[7] Liu XM, Lu GQ, Yan ZF, Beltramini J. Recent advances in catalysts for methanol synthesis via hydrogenation of CO and CO_2. Ind Eng Chem Res. 2003;42:6518–30.

[8] Dang S, Yang H, Gao P, Wang H, Li X, Wei W, et al. A review of research progress on heterogeneous catalysts for methanol synthesis from carbon dioxide hydrogenation. Catal Today. 2019;330:61–75.

[9] Catizzone E, Bonura G, Migliori M, Frusteri F, Giordano G. CO_2 recycling to dimethyl ether: state-of-the-art and perspectives. Molecules. 2018;23:31.

[10] Saravanan K, Ham H, Tsubaki N, Bae JW. Recent progress for direct synthesis of dimethyl ether from syngas on the heterogeneous bifunctional hybrid catalysts. Appl Catal B: Environ. 2017;217:494–522.

[11] Bonura G, Migliori M, Frusteri L, Cannilla C, Catizzone E, Giordano G, et al. Acidity control of zeolite functionality on activity and stability of hybrid catalysts during DME production via CO_2 hydrogenation. J CO_2 Util. 2018;24:398–406.

[12] Tan L, Zhang P, Cui Y, Suzuki Y, Li H, Guo L, et al. Direct CO_2 hydrogenation to light olefins by suppressing CO by-product formation. Fuel Process Technol. 2019;196:106174.

[13] Volkova G, Badmaev S, Belyaev V, Plyasova L, Budneva A, Paukshtis E, et al. Bifunctional catalysts for hydrogen production from dimethyl ether. Stud Surf Sci Catal. 2007;167:445–50.

[14] Badmaev SD, Akhmetov NO, Pechenkin AA, Sobyanin VA, Parmon VN. Low-temperature partial oxidation of dimethyl ether to hydrogen-rich gas over $CuO–CeO_2/\gamma\text{-}Al_2O_3$ catalysts for fuel cell supply. Doklady Phys Chem. 2019;487:95–8.

[15] Badmaev SD, Akhmetov NO, Belyaev VD, Kulikov AV, Pechenkin AA, Potemkin DI, et al. Syngas production via partial oxidation of dimethyl ether over $Rh/Ce_{0.75}Zr_{0.25}O_2$ catalyst and its application for SOFC feeding. Int J Hydrog Energy. 2020;45(49):26188–96. doi: 10.1016/j.ijhydene.2020.01.101.

[16] Shikada T, Ohno Y, Ogawa T, Ono M, Mizuguchi M. Direct synthesis of dimethyl ether form synthesis gas. Stud Surf Sci Catal. 1998;119:515–20.

[17] Frusteri F, Bonura G, Cannilla C, Ferrante GD, Aloise A, Catizzone E, et al. Stepwise tuning of metal-oxide and acid sites of CuZnZr-MFI hybrid catalysts for the direct DME synthesis by CO_2 hydrogenation. Appl Catal B: Environ. 2015;176:522–31.

[18] Ye J, Liu C, Mei D, Ge Q. Active oxygen vacancy site for methanol synthesis from CO_2 hydrogenation on In_2O_3 (110): a DFT study. ACS Catal. 2013;3:1296–306.

[19] Sun K, Fan Z, Ye J, Yan J, Ge Q, Li Y, et al. Hydrogenation of CO_2 to methanol over In_2O_3 catalyst. J CO_2 Util. 2015;12:1–6.

[20] Martin O, Martín AJ, Mondelli C, Mitchell S, Segawa TF, Hauert R, et al. Indium oxide as a superior catalyst for methanol synthesis by CO_2 hydrogenation. Angew Chem Int Ed. 2016;55:6109.

[21] Chen TY, Cao C, Chen TB, Ding X, Huang H, Shen L, et al. Unraveling highly tunable selectivity in CO_2 hydrogenation over bimetallic In–Zr oxide catalysts. ACS Catal. 2019;9:8785–97.

[22] Chou CY, Lobo RF. Direct conversion of CO_2 into methanol over promoted indium oxide-based catalysts. Appl Catal A: Gen. 2019;583:117144.

[23] Rui N, Wang Z, Sun K, Ye J, Ge Q, Liu CJ. CO_2 hydrogenation to methanol over Pd/In_2O_3: effects of Pd and oxygen vacancy. Appl Catal B: Environ. 2017;218:488–97.

[24] Snider JL, Streibel V, Hubert MA, Choksi TS, Valle E, Upham DC, et al. Revealing the synergy between oxide and alloy phases on the performance of bimetallic In–Pd catalysts for CO_2 hydrogenation to methanol. ACS Catal. 2019;9:3399–3412.

[25] Ham H, Baek SW, Shin CH, Bae JW. Roles of structural promoters for direct CO_2 hydrogenation to dimethyl ether over ordered mesoporous bifunctional $Cu/M–Al_2O_3$ (M = Ga or Zn). ACS Catal. 2018;9(1):679–90.

[26] Ham H, Kim J, Cho SJ, Choi JH, Moon DJ, Bae JW. Enhanced stability of spatially confined copper nanoparticles in an ordered mesoporous alumina for dimethyl ether synthesis from syngas. ACS Catal. 2016;6(9):5629–40.

[27] Tan L, Zhang P, Suzuki Y, Li H, Guo L, Yoneyama Y, et al. Bifunctional capsule catalyst of Al_2O_3@Cu with strengthened dehydration reaction field for direct synthesis of dimethyl ether from syngas. Ind Eng Chem Res. 2019;58(51):22905–11.

[28] Hu Y, Zhang Y, Du J, Li C, Wang K, Liu L, et al. The influence of composition on the functionality of hybrid $CuO–ZnO–Al_2O_3$/HZSM-5 for the synthesis of DME from CO_2 hydrogenation. RSC Adv. 2018;8(53):30387–95.

[29] Bonura G, Cannilla C, Frusteri L, Mezzapica A, Frusteri F. DME production by CO_2 hydrogenation: key factors affecting the behaviour of CuZnZr/ferrierite catalysts. Catal Today. 2017;281:337–44.

[30] Naik SP, Ryu T, Bui V, Miller JD, Drinnan NB, Zmierczak W. Synthesis of DME from CO_2/H_2 gas mixture. Chem Eng J. 2011;167:362–8.

[31] Bonura G, Cannilla C, Frusteri L, Catizzone E, Todaro S, Migliori M, et al. Interaction effects between CuO–ZnO–ZrO methanol phase and zeolite surface affecting stability of

hybrid systems during one-step CO_2 hydrogenation to DME. Catal Today. 2020;345:175–82.
[32] Witoon T, Kidkhunthod P, Chareonpanich M, Limtrakul J. Direct synthesis of dimethyl ether from CO_2 and H_2 over novel bifunctional catalysts containing CuO–ZnO–ZrO_2 catalyst admixed with WO_x/ZrO_2 catalysts. Chem Eng J. 2018;348:713–22.
[33] Bahruji H, Armstrong RD, Ruiz Esquius J, Jones W, Bowker M, Hutchings GJ. Hydrogenation of CO_2 to dimethyl ether over Brønsted acidic PdZn catalysts. Ind Eng Chem Res. 2018;57:6821–9.
[34] Glotov A, Vutolkina A, Pimerzin A, Vinokurov V, Lvov Y. Clay nanotube-metal core/shell catalysts for hydroprocesses. Chem Soc Rev. 2021;50:9240–77. doi: 10.1039/D1CS00502B.
[35] Lvov Y, Wang W, Zhang L, Fakhrullin R. Halloysite clay nanotubes for loading and sustained release of functional compounds. Adv Mater. 2016;28:1227–50.
[36] Lvov Y, Panchal A, Fu Y, Fakhrullin R, Kryuchkova M, Batasheva S, et al. Interfacial self-assembly in halloysite nanotube composites. Langmuir. 2019;35:8646–57.
[37] Vinokurov VA, Stavitskaya AV, Glotov AP, Novikov AA, Zolotukhina AV, Kotelev MS, et al. Nanoparticles formed onto/into halloysite clay tubules: architectural synthesis and applications. Chem Rec. 2018;18:858–67.
[38] Stavitskaya A, Glotov A, Mazurova K, Nedolivko V, Gushchin P, Huang W, et al. Formation of ruthenium nanoparticles inside aluminosilicate nanotubes and their catalytic activity in aromatics hydrogenation: the impact of complexing agents and reduction procedure. Pure Appl Chem. 2020;92:909–18.
[39] Glotov A, Vutolkina A, Pimerzin A, Nedolivko V, Zasypalov G, Stytsenko V, et al. Ruthenium catalysts templated on mesoporous MCM-41 type silica and natural clay nanotubes for hydrogenation of benzene to cyclohexane. Catalysts. 2020;10:537.
[40] Glotov A, Stavitskaya A, Chudakov Y, Ivanov E, Huang W, Vinokurov V, et al. Mesoporous metal catalysts templated on clay nanotubes. Bull Chem Soc Jpn. 2019;92:61–9.
[41] Glotov AP, Stavitskaya AV, Chudakov YA, Artemova MI, Smirnova EM, Demikhova NR, et al. Nanostructured ruthenium catalysts in hydrogenation of aromatic compounds. Pet Chem. 2018;58(14):1221–6.
[42] Vinokurov V, Glotov A, Chudakov Y, Stavitskaya A, Ivanov E, Gushchin P, et al. Core/shell Ruthenium–halloysite nanocatalysts for hydrogenation of phenol. Ind Eng Chem Res. 2017;56:14043–52.
[43] Afokin MI, Smirnova EM, Starozhitskaya AV, Gushchin PA, Glotov AP, Maksimov AL. Halloysite as a zeolite catalyst component for converting dimethyl ether into hydrocarbons. Chem Technol Fuels Oils. 2020;55:1–7.
[44] Vinokurov V, Stavitskaya A, Glotov A, Ostudin A, Sosna M, Gushchin P, et al. Halloysite nanotube-based cobalt mesocatalysts for hydrogen production from sodium borohydride. J Solid State Chem. 2018;268:182–9.
[45] Stavitskaya A, Mazurova K, Kotelev M, Eliseev O, Gushchin P, Glotov A, et al. Ruthenium-loaded halloysite nanotubes as mesocatalysts for fischer–tropsch synthesis. Molecules. 2020;25:1764.
[46] Glotov AP, Roldugina EA, Artemova MI, Smirnova EM, Demikhova NR, Stytsenko VD, et al. Isomerization of xylenes in the presence of pt-containing catalysts based on halloysite aluminosilicate nanotubes. Russ J Appl Chem. 2018;91(8):1353–62.
[47] Glotov AP, Artemova MI, Demikhova NR, Smirnova EM, Ivanov EV, Gushchin PA, et al. A study of platinum catalysts based on ordered Al–MCM-41 aluminosilicate and natural halloysite nanotubes in xylene isomerization. Pet Chem. 2019;2019(59):1226–34.
[48] Abbasov V, Mammadova T, Andrushenko N, Hasankhanova N, Lvov Y, Abdullayev E. Halloysite–Y-zeolite blends as novel mesoporous catalysts for the cracking of waste vegetable oils with vacuum gasoil. Fuel. 2014;117:552–5.
[49] Stavitskaya AV, Kozlova EA, Kurenkova AY, Glotov AP, Selischev DS, Ivanov EV, et al. Ru/CdS quantum dots templated on clay nanotubes as visible light active photocatalysts: optimization of S/Cd ratio and Ru content. Chem–A Eur J. 2020;26(57):13085–92. doi: 10.1002/chem.202002192.
[50] Vinokurov VA, Stavitskaya AV, Ivanov EV, Gushchin PA, Kozlov DV, Kurenkova AY, et al. Halloysite nanoclay based CdS formulations with high catalytic activity in hydrogen evolution reaction under visible light irradiation. ACS Sustain Chem Eng. 2017;5:11316–23.
[51] Liu R, Tian H, Yang A, Zha F, Ding J, Chang Y. Preparation of HZSM-5 membrane packed CuO–ZnO–Al_2O_3 nanoparticles for catalysing carbon dioxide hydrogenation to dimethyl ether. Appl Surf Sci. 2015;345:1–9.
[52] Wang Y, Wang W, Chen Y, Ma J, Li R. Synthesis of dimethyl ether from syngas over core–shell structure catalyst CuO–ZnO–Al_2O_3@SiO_2–Al_2O_3. Chem Eng J. 2014;250:248–56.
[53] Baktash E, Littlewood P, Schomäcker R, Thomas A, Stair PC. Alumina coated nickel nanoparticles as a highly active catalyst for dry reforming of methane. Appl Catal B: Environ. 2015;179:122–7.
[54] Abdalla A, Arudra P, Al-Khattaf SS. Catalytic cracking of 1-butene to propylene using modified H-ZSM-5 catalyst: a comparative study of surface modification and core-shell synthesis. Appl Catal A: Gen. 2017;533:109–20.
[55] Glotov A, Levshakov N, Stavitskaya A, Artemova M, Gushchin P, Ivanov E, et al. Templated self-assembly of ordered mesoporous silica on clay nanotubes. Chem Commun. 2019;55:5507–10.
[56] Paukshtis EA. IR spectroscopy for heterogeneous acid-base catalysis. Novosibirsk: Nauka; 1992.
[57] Bielz T, Lorenz H, Jochum W, Kaindl R, Klauser F, Klötzer B, et al. Hydrogen on In_2O_3: reducibility, bonding, defect formation, and reactivity. J Phys Chem C. 2010;114(19):9022–9.
[58] Martin O, Martín AJ, Mondelli C, Mitchell S, Segawa TF, Hauert R, et al. Indium oxide as a superior catalyst for methanol synthesis by CO_2 hydrogenation. Angew Chem Int Ed. 2016;55(21):6261–5.
[59] Yao L, Shen X, Pan Y, Peng Z. Unravelling proximity-driven synergetic effect within CIZO–SAPO bifunctional catalyst for CO_2 hydrogenation to DME. Energy Fuels. 2020;34(7):8635–43.
[60] Pustovarenko A, Dikhtiarenko A, Bavykina A, Gevers L, Ramírez A, Russkikh A, et al. Metal–organic framework-derived synthesis of cobalt indium catalysts for the hydrogenation of CO_2 to methanol. ACS Catal. 2020;10(9):5064–76.

Appendix

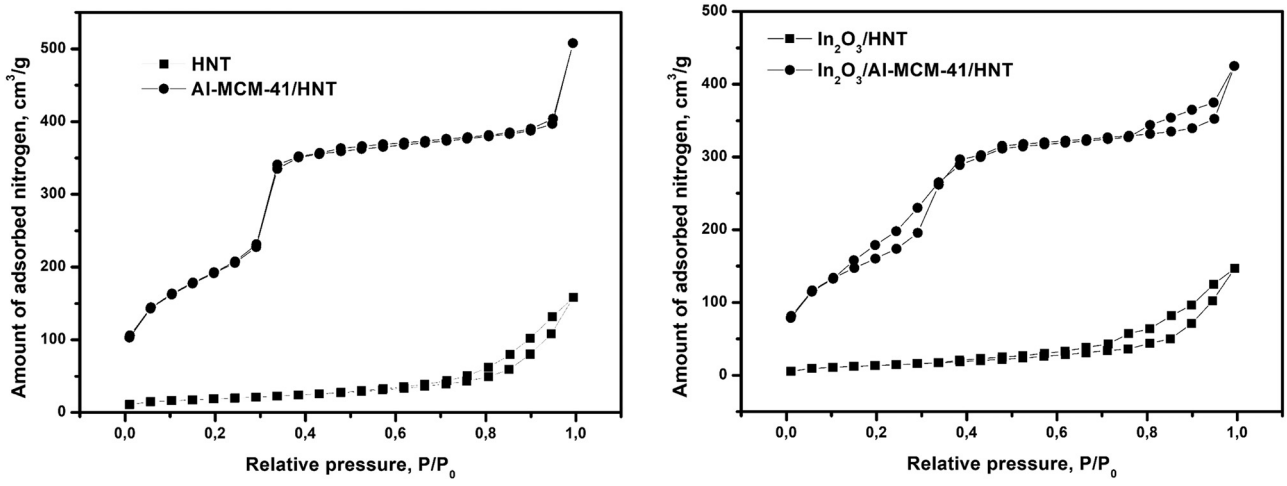

Figure A1: Low-temperature nitrogen adsorption isotherms for the HNT, Al-MCM-41/HNT, In_2O_3/HNT, and In_2O_3/Al–MCM-41/HNT samples.

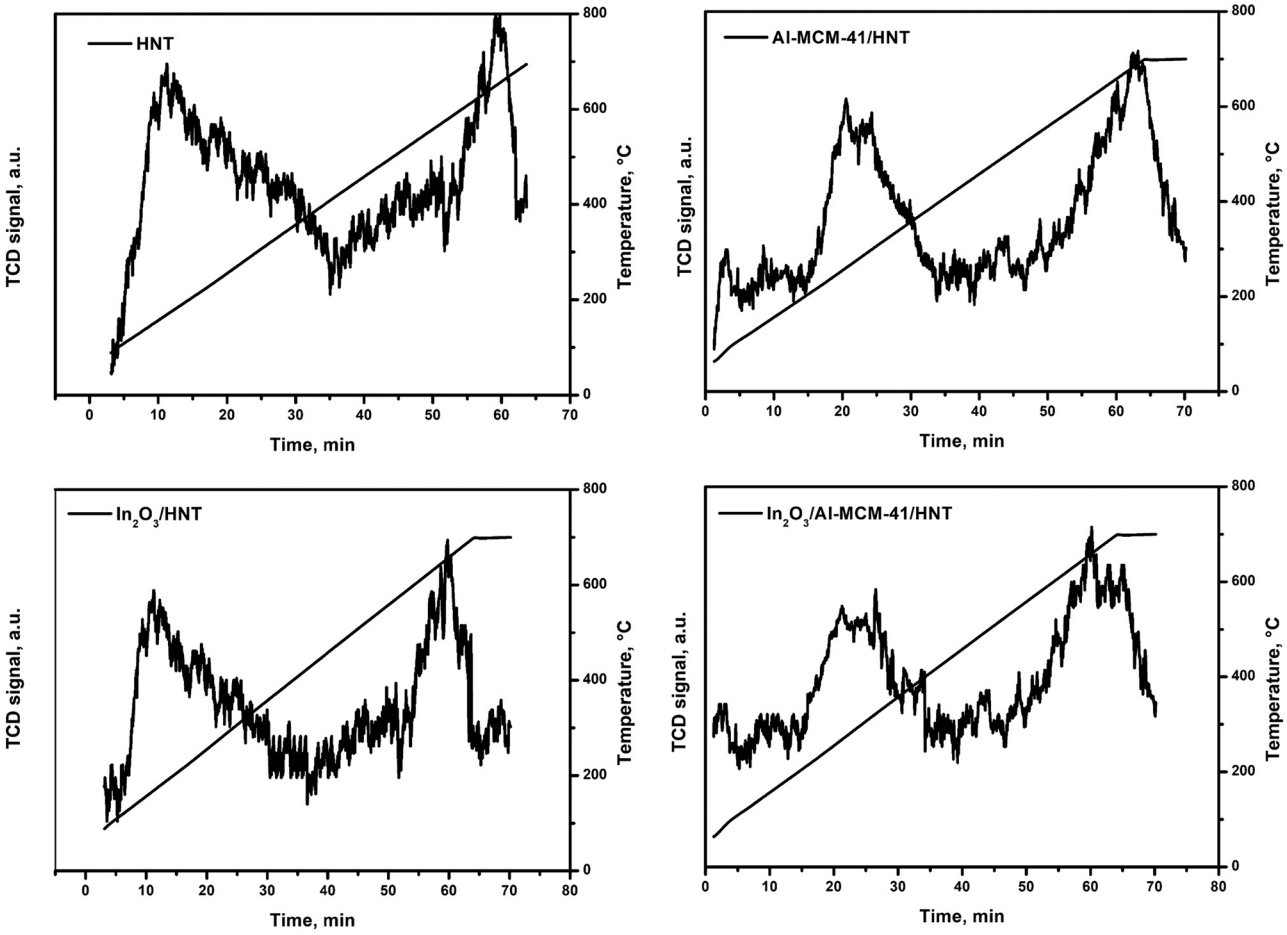

Figure A2: NH3-TPD curves for HNT, In_2O_3/HNT, Al-MCM-41/HNT, and In_2O_3/Al-MCM-41/HNT catalysts.